Steel and Composite Structures, *Vol. 31, No. 1 (2019) 43-51*
DOI: https://doi.org/10.12989/scs.2019.31.1.043

Computation of mixed-mode stress intensity factors in functionally graded materials by natural element method

J.R. Cho*

Department of Naval Architecture and Ocean Engineering, Hongik University, Sejong 30016, Korea

(*Received July 11, 2018, Revised March 9, 2019, Accepted March 17, 2019*)

Abstract. This paper is concerned with the numerical calculation of mixed-mode stress intensity factors (SIFs) of 2-D isotropic functionally graded materials (FGMs) by the natural element method (more exactly, Petrov-Galerkin NEM). The spatial variation of elastic modulus in non-homogeneous FGMs is reflected into the modified interaction integral $\tilde{M}^{(1,2)}$. The local NEM grid near the crack tip is refined, and the directly approximated strain and stress fields by PG-NEM are enhanced and smoothened by the patch recovery technique. Two numerical examples with the exponentially varying elastic modulus are taken to illustrate the proposed method. The mixed-mode SIFs are parametrically computed with respect to the exponent index in the elastic modulus and external loading and the crack angle and compared with the other reported results. It has been justified from the numerical results that the present method successfully and accurately calculates the mixed-mode stress intensity factors of 2-D non-homogeneous functionally graded materials.

Keywords: functionally graded materials (FGM); non-homogeneous material; mixed-mode stress intensity factor (SIF); modified interaction integral; near-tip grid refinement

1. Introduction

A functionally graded material (FGM) was introduced in the late 1980s to overcome the demerits of traditional layered heat-resisting composite materials (Apalak 2014). The thermal stress concentration at the layer interface, which was the most significant problem of layered heat-resisting composites, could be successfully reduced by inserting a graded layer between two different homogeneous material layers (Giannakopulos *et al*. 1995, Miyamoto *et al*. 2013). Here, a graded layer is meant by an inhomogeneous material layer in which the constituent particles of two homogeneous material layers are mixed up in a complex microstructure pattern (Reiter and Dvorak 1998, Vel and Goupee 2010). Besides the reduction of thermal stress concentration at the layer interface by removing the sharp material discontinuity, the thermo-mechanical performance of FGM could be maximized by appropriately tailoring the volume fraction distribution of constituent particles within the graded layer (Cho and Ha 2002).

In the beginning, most research efforts focused on the material characterization, thermo-mechanical analysis and fabrication (Noda 1999, Jabbari *et al*. 2002). But later, other mechanical behaviors, such as bending and buckling, vibration and fracture, were evaluated to expand the potential application fields of FGMs (Birman and Byrd 2007, Sidhoum *et al*. 2017, Khayat *et al*. 2017, Rizov 2017, Bouderba 2018). Bourada *et al*. (2019) investigated the dynamic responses of FG beam, and Zemri *et al*. (2015) and Bouafia et al. presented the nonlocal SDT and quasi-3D theory for studying the bending and free vibration responses of FG nanobeams. Bellifa *et al*. (2017) and Fourn *et al*. (2018) presented a novel four variable plate theory for the buckling and wave propagation analysis for FGM plates. Younsi *et al*. (2018) and Bounouara *et al*. (2016) presented a zero-order and 2, 3-D and zero-order SDTs for the free vibration analysis of FG- and FG-nanoscale plates, respectively. Abualnour *et al*. (2018) investigated the free vibration response of FGM plate by considering the thickness extension effect and Bourada *et al*. (2018) performed the stability analysis of S-FGM using a refined plate theory. Yahia *et al*. (2015) carried out the wave propagation analysis for FGM plate with porosities using higher-order shear deformation theory. Regarding FGM sandwich plates, Abdelaziz *et al*. (2017) and Meziane *et al*. (2014) presented a refined hyperbolic SDT for investigating bending, buckling and free vibration for various boundary conditions. El-Haina *et al*. (2017), Menasria *et al*. (2017) and Belabed *et al*. (2018) investigated the thermo-mechanical behaviors using the analytical approach and higher-order and hyperbolic SDTs, respectively.

Meanwhile, the thermo-mechanical behaviors of FGMs are influenced by the geometry, dimension, orientation and microstructure of constituent particles as well as the external loading and constraint. In particular, the structural failure of FGMs is dominated by micro-cracking because the microstructure is highly heterogeneous (Kawasaki and Watanabe 2002). In this context, the computation of stress intensity factors and the crack propagation simulation have been an important research subject (Dolbow and Gosz

*Corresponding author, Professor,
E-mail: jrcho@hongik.ac.kr

ISSN: 1229-9367 (Print), 1598-6233 (Online)

2002, Kim and Paulino 2002, Zhang *et al*. 2004, Tilbrook *et al*. 2005), in order to tailor FGMs which can be protected from the crack-driven failure.

One can employ traditional *J*–integral or interaction integrals for homogeneous materials. But, these standard integral methods provide path-dependent SIFs when applied to non-homogeneous materials. It is because the material properties vary point by point in non-homogeneous materials, but these standard integral methods cannot account for this spatial variation of material properties (Gu *et al*. 1999). The studies on the crack problems for non-homogeneous materials were initiated in the 1960~70s by assuming the spatial variation of the elastic modulus as an exponential function (Atkinson and List 1978, Dhaliwal and Singh 1978, Delale and Erdogan 1983). Eischen (1987) numerically investigated mixed-mode cracks in non-homogeneous materials by the finite element method, while Gu *et al*. (1999) presented a simplified method for calculating the crack-tip field of FGMs using the equivalent domain integral technique. Anlas *et al*. (2000) numerically evaluated SIFs in FGMs by discretizing the material property variation and by assigning different homogeneous elastic properties to each element. Kim and Paulino (2002) evaluated the mixed-mode SIFs in FGMs using FEM analysis with three different approaches: the path-independent $J_k^* -$ integral method, the modified crack-closure integral method, and the displacement correlation technique. Ayhan (2009) proposed the use of 3-D enriched finite elements to compute mixed-mode SIFs for 3-D cracks in elastic functionally graded materials. Mahbadi (2017) estimated stress intensity factors of rotating solid discs of cylinders with a radial crack.

Meanwhile, since the late 1990s, the application of meshfree methods to fracture mechanics problems has been actively progressed, in particular for the calculation of SIFs by the interaction integral, inspired by the fact that the interpolation functions used in meshfree methods provide high smoothness (Belytschko *et al*. 1995, Ching and Batra 2001, Brighenti 2005). The studies were not restricted to homogeneous materials but extended to non-homogeneous FGMs. Rao and Rahman (2003) and Liu *et al*. (2008) calculated both mode-I and mixed-mode SIFs of 2-D isotropic FGMs using element-free Galerkin (EFG) and meshless local Petrov-Galerkin (MLPG) methods, respectively. Wu and Liu (2016) developed a state space differential reproducing kernel (DRK) method for 3-D analysis of axisymmetric FGM plate.

However, these meshfree methods suffer from the common difficulties in the essential boundary condition enforcement and the numerical integration, because the interpolation functions do not obey the Kronecker delta property and the conventional Gauss quadrature rule cannot be directly employed (Sukumar *et al*. 1998, Cho and Lee 2006). Those difficulties not only require extra painstaking numerical techniques but also lead to the numerical deterioration. These shortcomings could be successfully resolved by the natural element method (NEM) (Braun and Sambridge 1995), particularly PG-NEM (Cho and Lee 2006), in which the interpolation functions called Laplace functions strictly obey the Kronecker delta property and the Delaunay triangles serve as a background cell for the numerical integration by the conventional Gauss quadrature rule.

As an extension of our previous work (Cho and Lee 2006, Cho 2016), this paper intends to extend the Petrov-Galerkin natural element method (PG-NEM) to the calculation of SIFs of 2-D isotropic functionally graded materials. Functionally graded materials are characterized by the non-uniformity of material properties over the material domain, and this spatial variation of the material properties is taken into consideration by the modified interaction integral $\widetilde{M}^{(1,2)}$. In order to increase the prediction accuracy of PG-NEM, the approximated strain and stress fields by NEM are enhanced by the recovery technique. In addition, NEM grid is locally refined in the vicinity of crack tip in order to maximize the grid point efficiency. Two numerical examples with exponentially varying elastic modulus and external loading are taken, and the mixed-mode SIFs are parametrically calculated with respect to the exponent index and the crack angle. The calculated SIFs are compared with the other reported values in order to justify the numerical accuracy and grid point efficiency of the proposed method.

2. Problem description

2.1 J̃–integral for 2-D isotropic FGM

Let us consider a 2-D linearly elastic and isotropic FGM shown in Fig. 1 with a crack inclined by α which occupies an open bounded domain $\Omega \in \Re^2$ with the boundary $\partial\Omega = \overline{\Gamma_D \cup \Gamma_N \cup \Gamma_c}$. Here, Γ_D denotes the displacement boundary, Γ_N the traction boundary, and $\Gamma_c = \overline{\Gamma_c^+ \cup \Gamma_c^-}$ the crack surface. FGMs are a representative inhomogeneous material such that the elastic modulus E and the Poison's ratio ν vary continuously on the material domain Ω. The material constants should be viewed as the effective ones in the macroscopic sense (Vel and Goupee 2010), because those are spatially discontinuous in the microscopic sense.

For mathematical description purpose, we use two Cartesian coordinate systems, $\{x, y\}$ for the 2-D linear elasticity problem and $\{x', y'\}$ for the stress intensity factor of angled crack respectively. Assuming the crack surface is

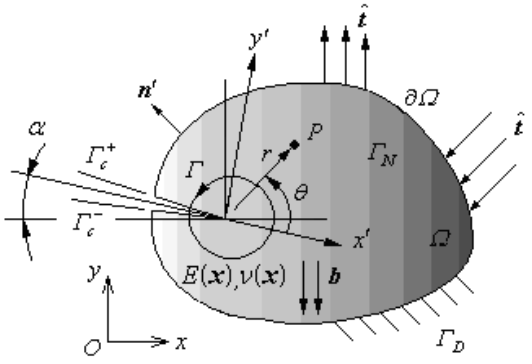

Fig. 1 A 2-D linear elastic FGM with an angled edge crack

traction-free and neglecting the body force $\boldsymbol{b}$, then the displacement field $\boldsymbol{u}(\boldsymbol{x})$ in the Cartesian coordinate system $\{x, y\}$ is governed by the static equilibrium

$$\nabla \cdot \sigma = 0 \quad in \quad \Omega \tag{1}$$

with the displacement boundary condition

$$\mathbf{u} = \hat{\mathbf{u}} \quad on \quad \Gamma_D \tag{2}$$

and the traction boundary condition given by

$$\sigma \cdot \mathbf{n} = \begin{cases} \hat{\mathbf{t}} \ on \ \Gamma_N \\ 0 \ on \ \Gamma_c^{\pm} \end{cases} \tag{3}$$

in which σ indicates the Cauchy stress and $\boldsymbol{n}$ the outward unit vector normal to $\partial\Omega$ and $\hat{\boldsymbol{t}}$ the surface force. By assuming small displacement and strains, the Cauchy strain ε is defined by the (3×2) gradient-like operator $\boldsymbol{L}$ such that

$$\varepsilon = \varepsilon(\mathbf{u}) = \mathbf{L}\mathbf{u} \tag{4}$$

Letting $\boldsymbol{D}$ be the constitutive tensor, the stresses and strains are constituted by

$$\sigma = \mathbf{D} : \varepsilon \tag{5}$$

Note that the displacement, strains and stresses are calculated based on the coordinate system $\{x, y\}$ and transformed into the coordinate system $\{x', y'\}$ using the chain rule and Mohr's circle.

For a homogeneous cracked body, the rate of released energy per unit crack extension in the x'–direction can be defined by the path-independent J–integral given by

$$J = \int_{\Gamma} \left(W\delta_{1j} - \sigma_{ij} \frac{\partial u_i}{\partial x_1'} \right) n_j' ds \tag{6}$$

using the indicial notation (i.e., $x_1' = x'$ and $x_2' = y'$). Here, $W = \boldsymbol{\sigma} \cdot \boldsymbol{\varepsilon} / 2 = \varepsilon_{ij} D_{ijkl} \varepsilon_{kl} / 2$ is the strain energy density and σ_{ij} are Cauchy stresses evaluated along an arbitrary contour Γ enclosing the crack tip in a counter-clock wise sense. Meanwhile, referring to Fig. 2, Γ is extended to $C = \Gamma + \Gamma_c^- + \Gamma_c^+ + \Gamma_o$ and a smooth weighting function

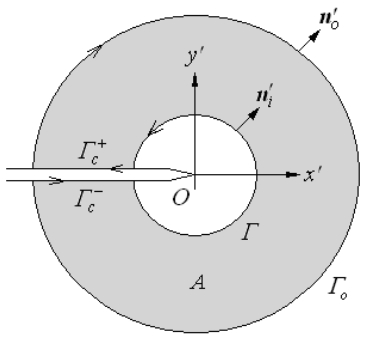

Fig. 2 An extended closed path C and the integral A

$q(\boldsymbol{x})(0 \le q \le 1)$ is introduced on the darkened domain A. The function q has unity on Γ, zero on Γ_o, and arbitrary value between 0 and 1 within the interior domain A. Then, taking the divergence theorem to Eq. (6) leads to

$$J = \int_A \left(\sigma_{ij} \frac{\partial u_i}{\partial x_1'} - W\delta_{1j} \right) \frac{\partial q}{\partial x_j'} dA + \int_A \frac{\partial}{\partial x_j'} \left(\sigma_{ij} \frac{\partial u_i}{\partial x_1'} - W\delta_{1j} \right) q dA \tag{7}$$

By expanding further the second term on the right hand side, Eq. (7) becomes

$$\begin{aligned} J = & \int_A \left(\sigma_{ij} \frac{\partial u_i}{\partial x_1'} - W\delta_{1j} \right) \frac{\partial q}{\partial x_j'} dA \\ & + \int_A \left(\frac{\partial \sigma_{ij}}{\partial x_j'} \frac{\partial u_i}{\partial x_1'} + \sigma_{ij} \frac{\partial^2 u_i}{\partial x_j' \partial x_1'} - \sigma_{ij} \frac{\partial \varepsilon_{ij}}{\partial x_1'} - \frac{1}{2} \varepsilon_{ij} \frac{\partial D_{ijkl}}{\partial x_1'} \varepsilon_{kl} \right) q dA \end{aligned} \tag{8}$$

All the terms in the second integrand in Eq. (8) vanish due to the equilibrium (1), compatibility (4) and the material homogeneity. Thus, the J–integral for homogeneous materials ends up with

$$J = \int_A \left(\sigma_{ij} \frac{\partial u_i}{\partial x_1'} - W\delta_{1j} \right) \frac{\partial q}{\partial x_j'} dA \tag{9}$$

in the area integral form. But, for inhomogeneous materials, the last material gradient term in the second integrand of Eq. (8) does not vanish. So, Eq. (8) reduces to the more general $\tilde{J}$ −integral (Gu *et al*. 1999), which is defined by

$$\tilde{J} = \int_A \left(\sigma_{ij} \frac{\partial u_i}{\partial x_1'} - W\delta_{1j} \right) \frac{\partial q}{\partial x_j'} dA - \int_A \frac{1}{2} \varepsilon_{ij} \frac{\partial D_{ijkl}}{\partial x_1'} \varepsilon_{kl} q dA \tag{10}$$

The second integral term becomes negligible as a contour Γ approaches to the crack tip, but it should be included for the relatively large integral domains.

2.2 Modified interaction integral $\tilde{M}^{(1,2)}$ for FGMs under mixed-mode loading

In order to extract K_I and K_{II} from J–integral, the interaction integral which considers two equilibrium states of a cracked body is employed. State 1 is the actual equilibrium state of a body subject to the prescribed boundary conditions while state 2 denotes an auxiliary equilibrium state which will be chosen as the asymptotic fields for modes I or II. In addition, another equilibrium state, called state S, can be led by superposing these two states, for which the $\tilde{J}$ −integral in Eq. (10) can be written as (Rao and Rahman 2000)

$$\begin{aligned} \tilde{J}^{(S)} = & \int_A \left(\left(\sigma_{ij}^{(1)} + \sigma_{ij}^{(2)} \right) \frac{\partial \left(u_i^{(1)} + u_i^{(2)} \right)}{\partial x_1'} - W^{(S)} \delta_{1j} \right) \frac{\partial q}{\partial x_j'} dA \\ & + \int_A \frac{\partial}{\partial x_j'} \left(\left(\sigma_{ij}^{(1)} + \sigma_{ij}^{(2)} \right) \frac{\partial \left(u_i^{(1)} + u_i^{(2)} \right)}{\partial x_1'} - W^{(S)} \delta_{1j} \right) q dA \end{aligned} \tag{11}$$

with

$$W^{(S)} = \frac{1}{2}\left(\sigma_{ij}^{(1)} + \sigma_{ij}^{(2)}\right)\left(\varepsilon_{ij}^{(1)} + \varepsilon_{ij}^{(2)}\right) = W^{(1)} + W^{(2)} + W^{(1,2)} \tag{12}$$

By utilizing the equilibrium (1) and the compatibility (4), Eq. (11) can be further simplified as

$$\begin{aligned}\tilde{J}^{(S)} &= \int_A \left(\left(\sigma_{ij}^{(1)} + \sigma_{ij}^{(2)}\right) \frac{\partial\left(u_i^{(1)} + u_i^{(2)}\right)}{\partial x_1'} - \left(W^{(1)} + W^{(2)} + W^{(1,2)}\right)\delta_{1j} \right) \frac{\partial q}{\partial x_j'} dA \\ &+ \int_A \frac{1}{2}\left(-\varepsilon_{ij}^{(1)} \frac{\partial D_{ijkl}}{\partial x_1'} \varepsilon_{kl}^{(1)} + \sigma_{ij}^{(1)} \frac{\partial \varepsilon_{ij}^{(2)}}{\partial x_1'} - \frac{\partial \sigma_{ij}^{(2)}}{\partial x_1'} \varepsilon_{ij}^{(1)} + \sigma_{ij}^{(2)} \frac{\partial \varepsilon_{ij}^{(1)}}{\partial x_1'} - \frac{\partial \sigma_{ij}^{(1)}}{\partial x_1'} \varepsilon_{ij}^{(2)} \right) q dA \\ &= \tilde{J}^{(1)} + \tilde{J}^{(2)} + \tilde{M}^{(1,2)}\end{aligned} \tag{13}$$

Here

$$\begin{aligned}\tilde{J}^{(1)} &= \int_A \left(\sigma_{ij}^{(1)} \frac{\partial u_i^{(1)}}{\partial x_1'} - W^{(1)}\delta_{1j} \right) \frac{\partial q}{\partial x_j'} dA \\ &- \frac{1}{2}\int_A \varepsilon_{ij}^{(1)} \frac{\partial D_{ijkl}}{\partial x_1'} \varepsilon_{kl}^{(1)} q dA\end{aligned} \tag{14}$$

$$\tilde{J}^{(2)} = \int_A \left(\sigma_{ij}^{(2)} \frac{\partial u_i^{(2)}}{\partial x_1'} - W^{(2)}\delta_{1j} \right) \frac{\partial q}{\partial x_j'} dA \tag{15}$$

are two $\tilde{J}$ −integrals for states 1 and 2, respectively, and

$$\begin{aligned}\tilde{M}^{(1,2)} &= \int_A \left(\sigma_{ij}^{(1)} \frac{\partial u_i^{(2)}}{\partial x_1'} + \sigma_{ij}^{(2)} \frac{\partial u_i^{(1)}}{\partial x_1'} - W^{(1,2)}\delta_{1j} \right) \frac{\partial q}{\partial x_j'} dA \\ &+ \int_A \frac{1}{2}\left(\sigma_{ij}^{(1)} \frac{\partial \varepsilon_{ij}^{(2)}}{\partial x_1'} - \frac{\partial \sigma_{ij}^{(2)}}{\partial x_1'} \varepsilon_{ij}^{(1)} + \sigma_{ij}^{(2)} \frac{\partial \varepsilon_{ij}^{(1)}}{\partial x_1'} - \frac{\partial \sigma_{ij}^{(1)}}{\partial x_1'} \varepsilon_{ij}^{(2)} \right) q dA\end{aligned} \tag{16}$$

is the modified interaction integral. All the quantities in Eq. (16) are evaluated with respect to a coordinate system originated at the crack tip, and the construction of the integral domain A and the weighting function $q(\boldsymbol{x})$ will be described in details in section 3.

According to Irwin's relation (Irwin 1957), the $\tilde{J}$ − integrals for linear elastic solids under mixed modes I and II also represents the energy release rate. Hence

$$\tilde{J}^{(1)} = \frac{1}{\bar{E}_{tip}}\left(K_I^{(1)^2} + K_{II}^{(1)^2} \right) \tag{17}$$

$$\tilde{J}^{(2)} = \frac{1}{\bar{E}_{tip}}\left(K_I^{(2)^2} + K_{II}^{(2)^2} \right) \tag{18}$$

and

$$\tilde{J}^{(S)} = \tilde{J}^{(1)} + \tilde{J}^{(2)} + \frac{2}{\bar{E}_{tip}}\left(K_I^{(1)} K_I^{(2)} + K_{II}^{(1)} K_{II}^{(2)} \right) \tag{19}$$

with $\bar{E}_{tip} = E_{tip}$ for plane stress and $\bar{E}_{tip} = E_{tip}/(1 - v^2)$ for plane strain at the crack tip. Equating Eqs. (13) and (19) leads to the following relation give by

$$\tilde{M}^{(1,2)} = \frac{2}{\bar{E}_{tip}}\left(K_I^{(1)} K_I^{(2)} + K_{II}^{(1)} K_{II}^{(2)} \right) \tag{20}$$

Referring to Anderson (1991), the closed form near-tip displacement fields for modes I and II in two-dimensional linear fracture mechanics are available. And, the mode I stress intensity factor $K_I^{(1)}$ for state 1 can be determined by making state 2 as the pure mode I asymptotic field (i.e., $K_I^{(2)} = 1$ and $K_{II}^{(2)} = 0$)

$$M^{(1,\text{Mode I})} = \frac{2}{\bar{E}_{tip}} K_I^{(1)} \tag{21}$$

In a similar manner, the stress intensity factor K_{II} of mode II can be also determined.

3. Computation of stress intensity factors by PG-NEM

3.1 Petrov-Galerkin natural element approximation

The boundary value problem (1) is converted to the weak form according to the virtual work principle: Find $\boldsymbol{u}(\boldsymbol{x})$ such that

$$\int_\Omega \varepsilon(\mathbf{v}) : \sigma(\mathbf{u}) d\Omega = \int_{\Gamma_N} \hat{\mathbf{t}} \cdot \mathbf{v}\, ds \tag{22}$$

for every admissible displacement field $\boldsymbol{v}(\boldsymbol{x})$ in the Cartesian coordinate system $\{x, y\}$. In order for the Petrov-Galerkin natural element approximation using a given non-convex natural element grid $\mathfrak{I}_{NEM}$ composed of N nodes and a number of Delaunay triangles as shown in Fig. 3(a), trial and test displacement fields $\boldsymbol{u}(\boldsymbol{x})$ and $\boldsymbol{v}(\boldsymbol{x})$ are expanded as

$$\mathbf{u}_h(\mathbf{x}) = \sum_{J=1}^{N} \mathbf{u}_J \phi_J(\mathbf{x}) = \Phi \bar{\mathbf{u}}, \qquad \mathbf{v}_h(\mathbf{x}) = \sum_{I=1}^{N} \mathbf{v}_I \psi_I(\mathbf{x}) = \Psi \bar{\mathbf{v}} \tag{23}$$

with Laplace interpolation functions $\phi_J(\boldsymbol{x})$ shown in Fig. 3(b) and CS-FE basis functions $\psi_I(\boldsymbol{x})$. The reader may refer to the references (Sukumar *et al*. 1998, Cho and Lee 2006) for more details on the CS-FE basis function and the concept of natural element method. Meanwhile, Φ and Ψ denote (2×2N) matrices containing N basis functions ϕ_J and ψ_I, and $\bar{\boldsymbol{u}}$ and $\bar{\boldsymbol{v}}$ are the (2N×1) nodal vectors, respectively.

Substituting Eq. (23) into Eqs. (4)-(5) and (22) leads to

$$\sum_I^N \mathbf{K}^I \bar{\mathbf{u}} = \sum_I^N \mathbf{F}^I \tag{24}$$

with the node-wise matrices defined by

$$\mathbf{K}^I = \int_{\Omega_v^I} (\mathbf{L}\Psi)^T \mathbf{D}(\mathbf{x})(\mathbf{L}\Phi) d\Omega \tag{25}$$

$$\mathbf{F}^I = \int_{\Gamma_N \cap \Omega_v^I} \Psi^T \hat{\mathbf{t}}\, ds \tag{26}$$

in which $\Omega_v^I = supp(\psi_I(\boldsymbol{x}))$ is the support of I-th CS-FE basis function (i.e., a Delaunay triangle), and two matrices Ψ and Φ are defined by

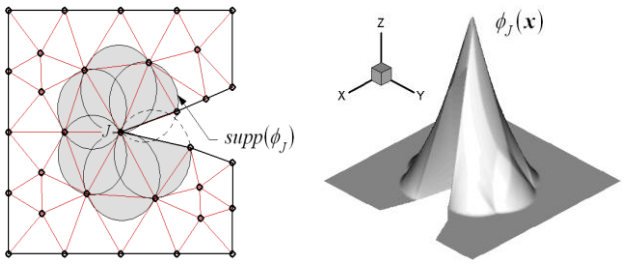

Fig. 3 (a) Non-convex NEM grid $\Im_{NEM}$; (b) laplace interpolation function $\phi_J(\boldsymbol{x})$ at the crack tip

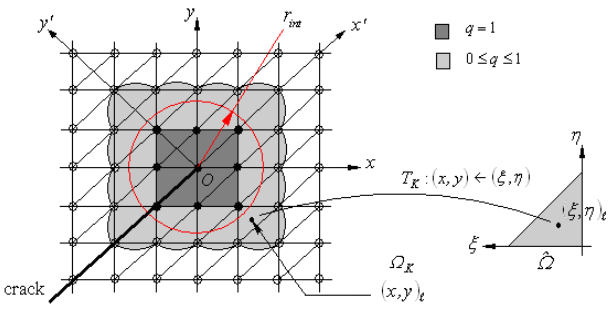

Fig. 4 Identification of the integral domain *A* and the weighting function $q(\boldsymbol{x})$

$$\Psi = \left[\begin{pmatrix} \psi_1 & 0 \\ 0 & \psi_1 \end{pmatrix} \cdots \begin{pmatrix} \psi_I & 0 \\ 0 & \psi_I \end{pmatrix} \cdots \begin{pmatrix} \psi_N & 0 \\ 0 & \psi_N \end{pmatrix} \right] \tag{27}$$

$$\Phi = \left[\begin{pmatrix} \phi_1 & 0 \\ 0 & \phi_1 \end{pmatrix} \cdots \begin{pmatrix} \phi_J & 0 \\ 0 & \phi_J \end{pmatrix} \cdots \begin{pmatrix} \phi_N & 0 \\ 0 & \phi_N \end{pmatrix} \right] \tag{28}$$

Furthermore, $\boldsymbol{L}$ is the (3×2) divergence-like operator defining Cauchy strains and $\boldsymbol{D}(\boldsymbol{x})$ indicates the position-dependent (3×3) material constant matrix of linear elasticity. The numerical integration in the natural element method is carried out Delaunay triangle by Delaunay triangle.

The Petrov-Galerkin natural element (PG-NE) method employs the Delaunay triangle-based CS-FE basis functions to expand the test displacement field. The main reason is to achieve both the numerical integration accuracy and the easy implementation of conventional Gauss quadrature rule (Cho and Lee 2006). The numerical integration in most meshfree methods is usually performed by applying the conventional Gauss quadrature rule to an extra background mesh which is additionally generated. But, differing from other meshfree methods, natural element method does not need additional effort to construct an extra background mesh because Delaunay triangles which are generated a priori in the process for defining the Laplace interpolation functions automatically construct a background mesh. Furthermore, the support of CS-FE basis functions is composed of a union of Delaunay triangles, so that the intersection region Ω_{int}^{IJ} between the CS-FE basis function ψ_I and Laplace basis function ϕ_J is always contained within Delaunay triangles. Therefore, one can accurately and easily integrate $\boldsymbol{K}^{\boldsymbol{I}}$ in Eq. (25) by applying the Gauss quadrature rule to each Delaunay triangle, as for the finite element method.

3.2 Natural element implementation of the modified interaction integral $\tilde{M}^{(1,2)}$

Referring to Fig. 4, the integral domain *A* and the weighting function $q(\boldsymbol{x})$ for the modified interaction integral (16) are constructed by specifying a radius r_{int} to identify an integral domain. The value of unity is assigned to all the nodes within the circle, while the value of zero is specified to the remaining nodes outside the circle within a whole NEM grid. Then, a union of interior darkened eight Delaunay triangles generates a rectangle and its boundary serves as an interior path Γ shown in the figure. In addition, one can define another union of grayed Delaunay triangles in which only one or two nodes in the triangles have the value of unity, and its boundary becomes the outer path Γ_o. Hence, the union of grayed Delaunay triangles automatically becomes the integral domain *A*, where the weighting function $q(\boldsymbol{x})$ defined in the Cartesian coordinate system $\{x, y\}$ has the value between zero and unity.

The gradient of weighting function $\partial q/\partial x_j'$ vanishes outside the integral domain *A*. So, let us denote M_A be the total number of grayed Delaunay triangles within the integral domain *A*. Then, the modified interaction integral (16) is integrated triangle by triangle such that

$$\tilde{M}^{(1,2)} = \sum_{K=1}^{M_A} \tilde{M}_K^{(1,2)} \tag{29}$$

with $\tilde{M}_K^{(1,2)}$ being the triangle-wise modified interaction integrals. Here, each triangle-wise interaction integral is computed by

$$\begin{aligned} \tilde{M}_e^{(1,2)} &= \int_{\Omega_K} \left[\sigma_{ij}^{(1)} \frac{\partial u_i^{(2)}}{\partial x_1'} + \sigma_{ij}^{(2)} \frac{\partial u_i^{(1)}}{\partial x_1'} - W^{(1,2)} \delta_{1j} \right] \frac{\partial q}{\partial x_j'} dA \\ &\quad + \frac{1}{2} \int_{\Omega_K} \left[\sigma_{ij}^{(1)} \frac{\partial \varepsilon_{ij}^{(2)}}{\partial x_1'} - \frac{\partial \sigma_{ij}^{(2)}}{\partial x_1'} \varepsilon_{ij}^{(1)} + \sigma_{ij}^{(2)} \frac{\partial \varepsilon_{ij}^{(1)}}{\partial x_1'} - \frac{\partial \sigma_{ij}^{(1)}}{\partial x_1'} \varepsilon_{ij}^{(2)} \right] q dA \\ &= \sum_{\ell=1}^{INT} \left\{ \left(\left[\sigma_{ij}^{(1)} \frac{\partial u_i^{(2)}}{\partial x_1'} + \sigma_{ij}^{(2)} \frac{\partial u_i^{(1)}}{\partial x_1'} - W^{(1,2)} \delta_{1j} \right] \frac{\partial q}{\partial x_j'} \Big|_{\mathbf{x}_\ell} \right) w_\ell |\mathbf{J}|_{\mathbf{x}_\ell} \right. \\ &\quad \left. + \frac{1}{2} \left[\sigma_{ij}^{(1)} \frac{\partial \varepsilon_{ij}^{(2)}}{\partial x_1'} - \frac{\partial \sigma_{ij}^{(2)}}{\partial x_1'} \varepsilon_{ij}^{(1)} + \sigma_{ij}^{(2)} \frac{\partial \varepsilon_{ij}^{(1)}}{\partial x_1'} - \frac{\partial \sigma_{ij}^{(1)}}{\partial x_1'} \varepsilon_{ij}^{(2)} \right] q(x_\ell) w_\ell |\mathbf{J}|_{\mathbf{x}_\ell} \right\} \end{aligned} \tag{30}$$

using the chain rule and Mohr's circle in order to transform the quantities in the NEM grid-oriented coordinates $\{x, y\}$ into those in the crack tip-aligned coordinates $\{x', y'\}$, as mentioned in Section 2.1. Meanwhile, *INT*, $\boldsymbol{x}_\ell$ and w_ℓ indicate the total number of integration points, sampling points and weights in conventional Gauss quadrate rule, respectively. Note that the sampling points $\boldsymbol{x}_\ell$ in Ω_K and the Jacobian $|\boldsymbol{J}|_{\boldsymbol{x}_\ell}$ are calculated using the geometry transformation T_K defined by

$$T_K : x_\ell = \sum_{i=1}^{3} x_i \psi_i(\xi,\eta)_\ell, \quad y_\ell = \sum_{i=1}^{3} y_i \psi_i(\xi,\eta)_\ell \tag{31}$$

between Ω_K in the coordinate system $\{x, y\}$ and the master triangle element $\widehat{\Omega}$. Here, $\{x_i, y_i\}$ are the co-ordinates of three grid points in each Delaunay triangle, $(\xi,\eta)_\ell$ the Gauss points in $\widehat{\Omega}$, and ψ_i the basis functions. For the current study, Laplace interpolation functions are used to interpolate the weighting function $q(\boldsymbol{x})$, and the points $\boldsymbol{x}_\ell$ in ϕ_K to compute these values are also determined by the geometry transformation (31). The strain and stress fields in state 1 are interpolated and recovered using Laplace interpolation functions ϕ_i $(\boldsymbol{x})$ and our patch recovery technique (2016). Meanwhile, in two-dimensional fracture problems, the displacement and stress fields at the tip of a mixed mode crack which are used for state 2 are given in a book by Anderson (1991).

4. Numerical experiments

We first consider a slant edge crack in a 2-D FGM plate in plane stress condition with the height H = 2 units and the width W = 1 unit. Referring to Fig. 5(a), the crack angle α is 45° and the relative crack length is $a/W = 0.4\sqrt{2}$. The Poison's ratio is kept constant with ν = 0.3, but the elastic modulus is assumed to be an exponential function in the x–direction, given by

$$E(x) = \bar{E}\exp[\eta(x-0.5)], \quad 0 \le x \le W \tag{32}$$

where, $\bar{E} = 1$ unit and ηa is variable for the parametric study such as ηa = 0, 0.1, 0.25, 0.5, 0.75 and 1.0. As external load, an exponentially varying distributed load is applied to the upper edge with $\sigma_{yy}(x,1) = \varepsilon\bar{E}\exp[\eta(x-0.5)]$ with $\bar{\varepsilon}$ being 1. All the bottom edge is constrained in the vertical direction (i.e., u_y = 0), and in addition the right end is constrained in the horizontal direction at the same time. A locally refined NEM grid shown in Fig. 5(b) is used, which is uniformly discretized by 10×22 and the near-tip region is locally refined with eight additional grid points. The total number of grid points is 244 because five additional grid points are needed along the crack to split a crack line into upper and lower lines. All the numerical integrations for the NEM analysis, the patch recovery and the modified interaction integral were performed using 13 Gassian points.

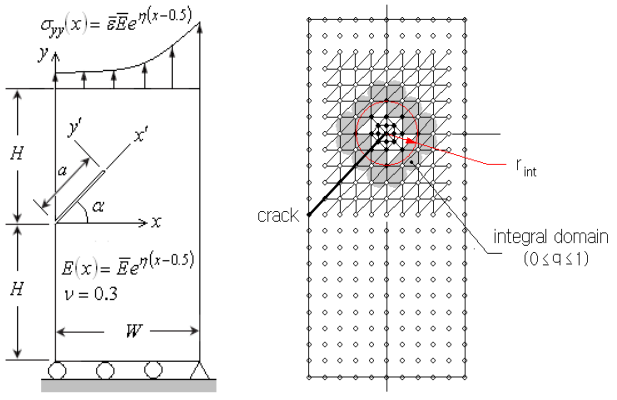

(a) (b)

Fig. 5 (a) A FGM plate with a slant edge crack under the exponentially varying distributed load; (b) a locally refined NEM grid and the integral domain (258 nodes)

Table 1 comparatively represents the predicted normalized SIFs $K_I/\bar{\varepsilon}\bar{E}\sqrt{\pi a}$ and $K_{II}/\bar{\varepsilon}\bar{E}\sqrt{\pi a}$ obtained for seven different ηa values. For the comparison purpose, the numerical results by Kim and Paulino (2002) and Rao and Rahman (2003) are also presented. It is noted that the FEM results by Kim and Paulino were obtained by the path-independent J_k^* – integral approach while the EFGM (element-free Galerkin method) results by Rao and Rahman were by the modified interaction integral $\widetilde{M}^{(1,2)}$. It is observed that the proposed method is in good agreement with FEM and EFGM such that the maximum relative difference is 4.01% at $K_{II}/\bar{\varepsilon}\bar{E}\sqrt{\pi a}$ for ηa = 0.25. Meanwhile, it is found that the present method provides slightly lower SIFs than FEM and EFGM at low ηa but the present method predicts slightly higher SIFs at high ηa.

Table 1 comparatively represents the predicted normalized SIFs $K_I/\bar{\varepsilon}\bar{E}\sqrt{\pi a}$ and $K_{II}/\bar{\varepsilon}\bar{E}\sqrt{\pi a}$ obtained for seven different ηa values. For the comparison purpose, the numerical results by Kim and Paulino (2002) and Rao and Rahman (2003) are also presented. It is noted that the FEM results by Kim and Paulino were obtained by the path-independent J_k^* – integral approach while the EFGM (element-free Galerkin method) results by Rao and Rahman were by the modified interaction integral $\widetilde{M}^{(1,2)}$. It is observed that the proposed method is in good agreement with FEM and EFGM such that the maximum relative difference is 4.01% at $K_{II}/\bar{\varepsilon}\bar{E}\sqrt{\pi a}$ for ηa = 0.25. Meanwhile, it is found that the present method provides slightly lower SIFs than FEM and EFGM at low ηa but the present method predicts slightly higher SIFs at high ηa.

Next, Fig. 6(a) shows an interior slant crack in a square FGM plate with the height and width $2H = 2W$ = 20 units. Konda and Erdogan (1994) have investigated an infinite plate such a configuration. The crack angle θ is set variable as given in Table 2 for the parametric computation, while the crack length is determined by $2a = 8/2\cos\theta$. The dependence of crack length on the crack angle is because the diagonal length of Delaunay triangles varies with the

Table 1 Normalized SIFs for a slanted crack in a functionally graded plate

ηa	Proposed method		Kim and Paulino $[J_k^*]$		Rao and Rahman $[\widetilde{M}^{(1,2)}]$	
	$\frac{K_I}{\bar{\varepsilon}\bar{E}\sqrt{\pi a}}$	$\frac{K_{II}}{\bar{\varepsilon}\bar{E}\sqrt{\pi a}}$	$\frac{K_I}{\bar{\varepsilon}\bar{E}\sqrt{\pi a}}$	$\frac{K_{II}}{\bar{\varepsilon}\bar{E}\sqrt{\pi a}}$	$\frac{K_I}{\bar{\varepsilon}\bar{E}\sqrt{\pi a}}$	$\frac{K_{II}}{\bar{\varepsilon}\bar{E}\sqrt{\pi a}}$
0.0	1.430	0.599	1.451	0.604	1.448	0.610
0.1	1.376	0.577	1.396	0.579	1.391	0.585
0.25	1.302	0.527	1.316	0.544	1.312	0.549
0.5	1.189	0.482	1.196	0.491	1.190	0.495
0.75	1.088	0.447	1.089	0.443	1.082	0.446
1.0	0.999	0.413	0.993	0.402	0.986	0.404

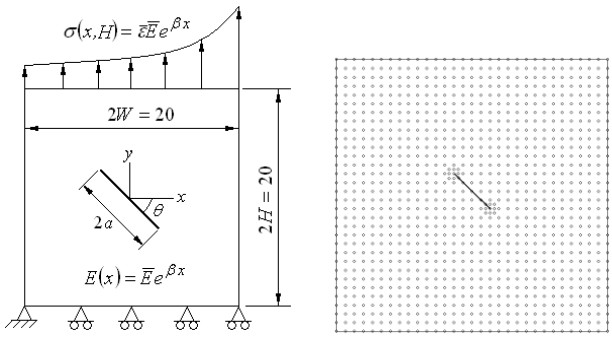

(a) (b)

Fig. 6 (a) A square plate with a slant center crack under an exponential tension load; (b) locally refined NEM grid (982 nodes)

crack angle. The grid-aligned Cartesian coordinates is positioned at the center of crack, and the crack angle is measured clockwise from the *x*–axis. The elastic modulus is assumed to be an exponential function given by

$$E(x)=\bar{E}\exp(\beta x),\quad -W\le x\le W \tag{33}$$

with $\bar{E}$ = 1 and $\beta = \eta a$. For the current problem, β is chosen as 0.25 and 0.5 while the Poisson's ratio is kept constant with ν = 0.3. The plate is assumed to be in plane stress condition and its upper edge is subjected to an exponentially varying distributed load $\sigma(x,H) = \bar{\varepsilon}\bar{E}\exp(\beta x)$ with $\bar{\varepsilon}$ = 1. Meanwhile, all the lower edge is constrained in the vertical direction (i.e., u_y = 0), and in addition, the horizontal constraint u_x = 0 is applied to the left end. This loading results in a uniform strain $\varepsilon_{yy}(x,y) = \bar{\varepsilon}$ in a corresponding uncracked plate.

Fig. 6(b) shows a locally refined NEM grid which was constructed by combining a 30×30 uniform grid and two near-tip refined grids. As in the previous examples, 13 Gaussian points were used for the NEM analysis, patch recovery, and the modified interaction integral. The normalized SIFs K_I/K_0 and K_I/K_0 at the left and right crack tips are given in Tables 2 and 3. From the comparison of

Table 2 Normalized stress intensity factors (ηa = 0.25, $K_0/\bar{\varepsilon}\bar{E}\sqrt{\pi a}$)

Method	θ/π	$K_I(-a)/K_0$	$K_{II}(-a)/K_0$	$K_I(+a)/K_0$	$K_{II}(+a)/K_0$
Proposed method	0	0.832	0	1.199	0
	0.1	0.787	-0.248	1.128	-0.314
	0.2	0.576	-0.405	0.830	-0.495
	0.3	0.288	-0.447	0.398	-0.510
	0.4	0.075	-0.283	0.121	-0.318
Konda and Erdogan	0	0.825	0	1.196	0
	0.1	0.750	-0.254	1.081	-0.321
	0.2	0.548	-0.422	0.784	-0.514
	0.3	0.290	-0.437	0.414	-0.504
	0.4	0.075	-0.282	0.121	-0.304

Table 3 Normalized stress intensity factors (ηa = 0.5, $K_0/\bar{\varepsilon}\bar{E}\sqrt{\pi a}$)

Method	θ/π	$K_I(-a)/K_0$	$K_{II}(-a)/K_0$	$K_I(+a)/K_0$	$K_{II}(+a)/K_0$
Proposed method	0	0.680	0	1.533	0
	0.1	0.640	-0.218	1.373	-0.335
	0.2	0.471	-0.336	0.943	-0.532
	0.3	0.246	-0.404	0.451	-0.547
	0.4	0.068	-0.271	0.137	-0.341
Konda and Erdogan	0	0.674	0	1.424	0
	0.1	0.617	-0.213	1.285	-0.344
	0.2	0.460	-0.365	0.925	-0.548
	0.3	0.247	-0.397	0.490	-0.532
	0.4	0.059	-0.269	0.146	-0.314

Tables 4 and 5, it is found that the case of ηa = 0.25 leads to higher normalized SIFs than the case of ηa = 0.5 for the left crack tip and vice versa for the right crack tip. This is because the slope of exponential tension load increases in proportional to the value of $\beta = \eta a$. It is confirmed that the proposed method is in a reasonable agreement with Konda and Erdogan (1994) for all the crack angles. The maximum relative difference is found to be 7.96% at $K_I(+a)/K_0$ for θ/π = 0.3 and ηa = 0.5. They considered an infinite plate with an interior slant crack but our plate model is finite, which is one of error sources.

5. Conclusions

This paper presented an extension of PG-NEM to the evlaluation of mixed-mode stress intensity factors (SIF) in 2-D functionally graded materials (FGM). In PG-NEM, Voronoi polygon-based Laplace interpolation functions and Delaunay triangle-based CS-FEM functions were used as trial and test basis functions, respectively, for the sake of effective and accurate implementation of essential boundary condition and the numerical integration. The modified interaction integral $\tilde{M}^{(1,2)}$ has been implemented into PG-NEM to account for the spatial variation of the elastic modulus of non-homogeneous FGMs. In addition, the patch recovery technique and the neat-tip local grid refinement has been introduced to obtain more accurate and smoothened strain and stress fields.

Two numerical examples for evaluating the mixed-mode SIFs were parametrically investigated in order to illustrate and validate the proposed method. A slant edge crack and an interior slant crack under exponentially varying tensile loading were considered. The elastic modulus was assumed to be an exponential function of the horizontal co-ordinate and the corresponding index as well as the crack angle was taken as a parametric variable. The proposed method was compared with the J_k^*-integral using FEM and the modified interaction integral $\left[\tilde{M}^{(1,2)}\right]$ using EFGM as well as the analytical approach. From the comparison, the numerical accuracy and the grid point efficiency of the proposed method have been justified such that the

maximum relative difference is less than 5% for the first example and less than 8% for the second example, for the locally near-tip refined coarse NEM grids.

Acknowledgments

This research was supported by Basic Science Research Program through the National Research Foundation of Korea (NRF) funded by the Ministry of Education (Grant No. NRF-2017R1D1A103028879).

References

Abdelaziz, H.H., Meziane, M.A.A., Bousahla, A.A., Tounsi, A., Mahmoud, S.R. and Alwabli, A.S. (2017), "An efficient hyperbolic shear deformation theory for bending, buckling and free vibration of FGM sandwich plates with various boundary conditions", *Steel Compos. Struct., Int. J.*, **25**(6), 693-704.

Abualnour, M., Houari, M.S.A., Tounsi, A., Bedia, E.A.A. and Mahmoud, S.R. (2018), "A novel quasi-3D trigonometric plate theory for free vibration analysis of advanced composite plates", *Compos. Struct.*, **184**, 688-697.

Anderson, T.L. (1991), *Fracture Mechanics: Fundamentals and Applications*, (1st Edition), CRC Press.

Anlas, G., Santare, M.H. and Lambros, J. (2000), "Numerical calculation of stress intensity factors in functionally graded materials", *Int. J. Fracture*, **104**, 131-143.

Apalak, M.K. (2014), "Functionally graded adhesively bonded joints", *Rev. Adhesion Adhesive*, **1**, 56-84.

Atkinson, C. and List, R.D. (1978), "Steady state crack propagation into media with spatially varying elastic properties", *Int. J. Eng. Sci.*, **16**, 717-730.

Ayhan, A.O. (2009), "Three-dimensional mixed-mode stress intensity factors for cracks in functionally graded materials using enriched finite elements", *Int. J. Solids Struct.*, **46**(3-4), 796-810.

Belabed, Z., Bousahla, A.A., Houari, M.S.A., Tounsi, A. and Mahmoud, S.R. (2018), "A new 3-unknown hyperbolic shear deformation theory for vibration of functionally graded sandwich plate", *Earthq. Struct., Int. J.*, **14**(2), 103-115.

Bellifa, H., Bakora, A., Tounsi, A., Bousahla, A.A. and Mahmoud, S.R. (2017), "An efficient and simple four variable refined plate theory for buckling analysis of functionally graded plates", *Steel Compos. Struct., Int. J.*, **25**(3), 257-270.

Belytschko, T., Lu, Y.Y., Gu, L. and Tabbara, M. (1995), "Element-free Galerkin methods for static and dynamic fracture", *Int. J. Solids Struct.*, **32**(17-18), 2547-2570.

Birman, V. and Byrd, L.W. (2007), "Modeling and analysis of functionally graded materials and structures", *Appl. Mech. Rev.*, **60**(5), 195-216.

Bouafia, K., Kaci, A., Houari, M.S.A., Benzair, A. and Tounsi, A. (2017), "A nonlocal quasi-3D theory for bending and free flexural vibration behaviors of functionally graded nanobeams", *Smart Struct. Syst., Int. J.*, **19**(2), 115-126.

Bouderba, B. (2018), "Bending of FGM rectangular plates resting on non-uniform elastic foundations in thermal environmental using an accurate theory", *Steel Compos. Struct., Int. J.*, **27**(3), 311-325.

Bounouara, F., Benrahou, K., Belkorissat, I. and Tounsi, A. (2016), "A nonlocal zeroth-order shear deformation theory for free vibration of functionally graded nanoscale plates resting on elastic foundation", *Steel Compos. Struct., Int. J.*, **20**(2), 227-249.

Bourada, F., Amara, K., Bousahla, A.A., Tounsi, A. and Mahmoud, S.R. (2018), "A novel refined plate theory for stability analysis of hybrid and symmetric S-FGM plates", *Struct. Eng. Mech., Int. J.*, **68**(6), 661-675.

Bourada, F., Bousahla, A.A., Bourada, M., Azzaz, A., Zinata, A. and Tounsi, A. (2019), "Dynamic investigation of porous functionally graded beam using a sinusoidal shear deformation theory", *Wind Struct., Int. J.*, **28**(1) 19-30.

Braun, J. and Sambridge, M. (1995), "A numerical method for solving partial differential equations on highly irregular evolving grids", *Nature*, **376**, 655-660.

Brighenti, R. (2005), "Application of the element-free Galerkin meshless method to 3-D fracture mechanics problems", *Eng. Fract. Mech.*, **72**, 2808-2820.

Ching, H.K. and Batra, R.C. (2001), "Determination of crack tip fields in linear elastostatics by the meshless local Petrov-Galerkin (MLPG) method", *Comput. Model. Eng. Sci.*, **2**(2), 273-289.

Cho, J.R. (2016), "Stress recovery techniques for natural element method in 2-D solid mechanics", *J. Mech. Sci. Technol.*, **30**(11), 5083-5091.

Cho, J.R. and Ha, D.Y. (2002), "Optimal tailoring of 2D volume-fraction distributions for heat-resisting functionally graded materials using FDM", *Comput. Methods Appl. Mech. Engrg.*, **191**, 3195-3211.

Cho, J.R. and Lee, H.W. (2006), "A Petrov-Galerkin natural element method securing the numerical integration accuracy", *J. Mech. Sci. Technol.*, **20**(1), 94-109.

Delale, F. and Erdogan, F. (1983), "The crack problem for a nonhomogeneous plane", *J. Appl. Mech.*, **50**, 609-614.

Dhaliwal, R.S. and Singh, B.M. (1978), "On the theory of elasticity of a nonhomogeneous medium", *Int. J. Elasticity*, **8**, 211-219.

Dolbow, J.E. and Gosz, M. (2002), "On the computation of mixed-mode stress intensity factors in functionally graded materials", *Int. J. Solids Struct.*, **39**(9), 2557-2574.

Eischen, J.W. (1987), "Fracture of nonhomogeneous materials", *Int. J. Fracture*, **34**, 3-22.

El-Haina, F., Bakora, A., Bousahla, A.A., Tounsi, A. and Mahmoud, S.R. (2017), "A simple analytical approach for thermal buckling of thick functionally graded sandwich plates", *Struct. Eng. Mech., Int. J.*, **63**(5), 585-595.

Fourn, H., Atmane, H.A., Bourada, M., Bousahla, A.A., Tounsi, A. and Mahmoud, S.R. (2018), "A novel four variable refined plate theory for wave propagation in functionally graded materials plates", *Steel Compos. Struct., Int. J.*, **27**(1), 109-122.

Giannakopulos, A.E., Suresh, S. and Olsson, M. (1995), "Elastoplastic analysis of thermal cycling: layered materials with compositional gradients", *Acta Metall. Mater.*, **43**(4), 1335-1354.

Gu, P., Dao, M. and Asaro, R.J. (1999), "A simplified method for calculating the crack tip field of functionally graded materials using the domain integral", *J. Appl. Mech.*, **66**(1), 101-108.

Irwin, G.R. (1957), "Analysis of stresses and strains near the end of a crack traveling a plate", *J. Appl. Mech.*, **24**, 361-364.

Jabbari, M., Sohrabpour, S. and Eslami, M.R. (2002), "Mechanical and thermal stresses in a functionally graded hollow cylinder due to radially symmetric loads", *Int. J. Pressure Vessel. Piping*, **79**(1), 493-497.

Kawasaki, K. and Watanabe, R. (2002), "Thermal fracture behavior of metal/ceramic functionally graded materials", *Eng. Fract. Mech.*, **69**(14-16), 1713-1728.

Khayat, M., Poorveis, D. and Moradi, S. (2017), "Buckling analysis of functionally graded truncated conical shells under external displacement-dependent pressure", *Steel Compos. Struct., Int. J.*, **23**(1), 1-16.

Kim, J.H. and Paulino, G.H. (2002), "Finite element evaluation of mixed mode stress intensity factors in functionally graded

materials", *Int. J. Numer. Methods Eng.*, **53**, 1903-1935.
Konda, N. and Erdogan, F. (1994), "The mixed mode crack problem in a non-homogeneous elastic medium", *Eng. Fract. Mech.*, **47**(4), 533-545.
Liu, K.Y., Long, S.Y. and Li, G.Y. (2008), "A meshless local Petrov-Galerkin method for the analysis of cracks in the isotropic functionally graded material", *Comput. Model. Eng. Sci.*, **7**(1), 43-57.
Mahbadi, H. (2017), "Stress intensity factor of radial cracks in isotropic functionally graded solid cylinders", *Eng. Fract. Mech.*, **180**, 115-131.
Menasria, A, Bouhadra, A., Tounsi, A., Bousahla, A.A. and Mahmoud, S.R. (2017), "A new simple HSDT for thermal stability analysis of FG sandwich plates", *Steel Compos. Struct., Int. J.*, **25**(2), 157-175.
Meziane, M.A.A., Abdelaziz, H.H. and Tounsi, A. (2014), "An efficient and simple refined theory for buckling and free vibration of exponentially graded sandwich plates under various boundary conditions", *J. Sandw. Struct. Mater.*, **16**(3), 293-318.
Miyamoto, Y., Kaysser, W.A., Rabin, B.H. and Kawasaki, A. (2013), *Functionally Graded Materials: Design. Processing and Applications*, Springer Science & Business Media.
Noda, N. (1999), "Thermal stresses in functionally graded materials", *J. Thermal Stress.*, **22**(4-5), 477-512.
Rao, B.N. and Rahman, S. (2000), "An efficient meshless method for fracture analysis of cracks", *Comput. Mech.*, **26**, 398-408.
Rao, B.N. and Rahman, S. (2003), "Mesh-free analysis of cracks in isotropic functionally graded materials", *Eng. Fract. Mech.*, **70**, 1-27.
Reiter, T. and Dvorak, G.J. (1998), "Micromechanical models for graded composite materials: II. Thermomechanical loading", *J. Phys. Solids*, **46**(9), 1655-1673.
Rizov, V.I. (2017), "Fracture analysis of functionally graded beams with considering material nonlinearity", *Struct. Eng. Mech., Int. J.*, **64**(4), 487-494.
Sidhoum, I.A., Boutchicha, D., Benyoucef, S. and Tounsi, A. (2017), "An original HSDT for free vibration of functionally graded plates", *Steel Compos. Struct., Int. J.*, **25**(6), 735-745.
Sukumar, N., Moran, A. and Belytschko, T. (1998), "The natural element method in solid mechanics", *Int. J. Numer. Methods Eng.*, **43**, 839-887.
Tilbrook, M.T., Moon, R.J. and Hoffman, M. (2005), "Crack propagation in graded composites", *Compos. Sci. Technol.*, **65**(2), 201-220.
Vel, S.S. and Goupee, A.J. (2010), "Multiscale thermoelastic analysis of random heterogeneous materials, Part I: microstructure characterization and homogenization of material properties", *Comput. Mater. Sci.*, **48**, 22-38.
Wu, C.P. and Liu, Y.C. (2016), "A state space meshless method for the 3D analysis of FGM axisymmetric circular plates", *Steel Compos. Struct., Int. J.*, **22**(1), 161-182.
Yahia, S.A., Atmane, H.A., Houari, M.S.A. and Tounsi, A. (2015), "Wave propagation in functionally graded plates with porosities using various higher-order shear deformation plate theories", *Struct. Eng. Mech., Int. J.*, **53**(6), 1143-1165.
Younsi, A., Tounsi, A., Zaoui, F.Z., Bousahla, A. and Mahmoud, S.R. (2018), "Novel quasi-3D and 2D shear deformation theories for bending and free vibration analysis of FGM plates", *Geomech. Eng., Int. J.*, **14**(6), 519-532.
Zemri, A., Houari, M.S.A., Bousahla, A.A. and Tounsi, A. (2015), "A mechanical response of functionally graded nanoscale beam: an assessment of a refined nonlocal shear deformation theory beam theory", *Struct. Eng. Mech., Int. J.*, **54**(4), 693-710.
Zhang, Ch., Sladek, J. and Sladek, V. (2004), "Crack analysis in unidirectionally and bidirectionally functionally graded materials", *Int. J. Fract.*, **129**, 385-406.